J. Fluid Mech. (2012), *vol.* 702, *pp.* 470–487. © Cambridge University Press 2012
doi:10.1017/jfm.2012.200

Global vorticity shedding for a shrinking cylinder

G. D. Weymouth[1]† **and M. S. Triantafyllou**[2]

[1] Singapore–MIT Alliance for Research and Technology Centre, S16-05-08 3 Science Drive 2, Singapore 117543

[2] Center for Ocean Engineering, Massachusetts Institute of Technology, 77 Massachusetts Avenue, Cambridge, MA 02139, USA

(Received 7 October 2011; revised 28 March 2012; accepted 19 April 2012; first published online 7 June 2012)

We study numerically the viscous flow around a steadily moving two-dimensional cylinder undergoing a rapid reduction in its diameter as a model problem for force production through shape change which is encountered in the locomotion of certain animals. We consider first the case of a rapidly collapsing circular cylinder in steady translation, starting from an original diameter and reaching a final, smaller diameter under prescribed kinematics. We show that the difference in added mass energy is recovered by the body, and the boundary layer vorticity is reduced through annihilation with opposite-sign vorticity generated during the reduction phase. Next we consider a steadily moving circular cylinder which undergoes rapid but orderly melting, resulting in the same reduction of its diameter but which exhibits radically different flow patterns compared to the collapsing cylinder. The original vorticity in the boundary layer is shed instantaneously and globally in the fluid at the start of the melting phase, and then rapidly rolls up to form a pair of strong vortices, which contain the energy difference between the original and final cylinder states. The formation of the vortices in the melting cylinder takes less than a third of the time required by a rigid translating cylinder to form such vortices.

Key words: propulsion, vortex shedding

1. Introduction

Aquatic and aerial animals move through unsteady motion of their bodies and fins. They impart kinetic energy and momentum to the fluid in modes that are presumed to have been optimized through evolution. Of particular interest is locomotion that involves significant shape change. The fins of small fish are flexible and undergo shape change during a cycle of oscillation (Drucker & Lauder 2000; Ramamurti *et al.* 2002; Dong *et al.* 2010). Childress, Vandenberghe & Zhang (2006) studied a body with variable frontal area exposed to an oscillatory flow, and showed that it can suspend itself against gravity by taking advantage of the change in added mass between upstroke and downstroke. Similarly, Spagnolie & Shelley (2009) showed that a two-dimensional cylinder with variable frontal area within an oscillatory flow can propel itself by appropriate active phase control of its shape change. Johansson & Norberg

† Email address for correspondence: weymouth@mit.edu

https://doi.org/10.1017/jfm.2012.200 Published online by Cambridge University Press

(2003) studied the shape change of the duck's foot from a drag orientation to a lift orientation, resulting in shedding of vorticity. Similarly, water striders at the interface between air and water (Dickinson 2003) impart momentum to the fluid when the legs move from water to air, forming propulsive vortex structures. Hsieh & Lauder (2004) found that basilisk lizards running on the water surface impart vorticity from their feet into the water to produce dynamic lift and support their weight (Hu & Bush 2010). Dong *et al.* (2010) studied a pectoral fin undergoing active or passive deformations during the paddling stroke, finding significant improvement in thrust compared to a rigid fin. Bats have flexible wings, capable of changing shape (Hedenstrom, Johansson & Spedding 2006; Lindhe Norberg & Winter 2006).

When a body is accelerated within a viscous fluid, it conveys kinetic energy and momentum to the fluid, while vorticity is generated at its surface and contained in its boundary layer. The boundary layer may separate to generate vortical patterns, further altering the kinetic energy and momentum of the fluid (Williamson 1996). When a moving body suddenly stops or is decelerated to reach a lower speed, or undergoes rapid shape change, some of the fluid energy may be recovered and some remains in the fluid, while the vorticity of the boundary layer undergoes rapid changes as part, or all, of the original vorticity may be shed into the fluid; in the latter case the questions raised are what fluid patterns form, what the time constants are, and how fluid energy redistributes and changes.

Taylor (1953) studied analytically the problem of an impulsively accelerated circular disk of vanishing thickness moving in the direction perpendicular to the disk surface; the disk suddenly disappears or melts totally. A potential flow was employed, but a shear layer was assumed to form at the location of the melted disk. Using conservation of energy, impulse and circulation, and further assuming that the freed vorticity will form a single vortex ring of uniform core, Taylor determined the resulting vortex ring strength and diameter.

Fohl (1968) considered analytically the rapid acceleration of a sphere of fluid; the flow shear at the surface of the sphere is modelled as a sheet of vortex rings, which is assumed to evolve into a single vortex ring, retaining the impulse and kinetic energy of the originally generated flow field. Eames (2008*a*) studied moving vapour bubbles which condense, or moving droplets undergoing a phase change, the equivalent of (fluid) 'bodies' disappearing, leaving behind them 'ghost' vortices.

Eames (2008*b*) considered the rapid (total) dissolution of a dense body in an inviscid fluid. As the body dissolves, the bound vorticity is pushed into the ambient flow by the density gradient, creating free vorticity, which eventually generates a dipolar vortex in the case of a dissolving cylinder, and a vortex ring in the case of a sphere. In the case of a body of equal density with the fluid, the potential flow is unchanged by the dissolving body, owing to the lack of viscous effects.

We consider computationally a problem similar to the melting disk of Taylor (1953) and the dissolving body of Eames (2008*b*), that can serve as a simple model for force and vortex production through shape change: a two-dimensional circular cylinder is first rapidly accelerated from rest within a viscous fluid to reach a constant speed, and then undergoes a rapid shape change, retaining its circular shape but reducing its diameter by 20 %. We study the changes in the force, fluid kinetic energy, and vorticity induced by two manners of rapidly shrinking the cylinders: first a shape *collapse* with prescribed kinematics, and second a prescribed *melting* resulting in a smaller diameter cylinder. These results are compared to the initial vortex formation on a constant-diameter cylinder, as well as to potential flow predictions. Radically different results are obtained for the two cases studied.

https://doi.org/10.1017/jfm.2012.200 Published online by Cambridge University Press

We choose a viscous two-dimensional model of shape change, because it allows us to investigate the problem very efficiently while enabling an assessment of the importance of viscous effects. We impose the initial acceleration from rest, as well as the cylinder size reduction, to occur within a short time, so that flow separation is limited and the flow does not form a sizable wake. This allows us to see more clearly the flow patterns resulting from the shape change, particularly with respect to the shed vorticity and the subsequently forming vortical patterns.

The rapid change in the shape of the body causes a corresponding reduction in the cylinder added mass and its related kinetic energy; as we show in the paper, the balance of kinetic energy is either released from the body into the wake, or recovered at the body surface through the applied force. Hence, inertia forces are dominant, while the vorticity, starting from its generation at the boundary layer to the shedding in the flow, accompanies the rapid changes in the flow, rather than causing them. Hence there is a basic difference with, for example, the formation of the wake behind a cylinder, where boundary layer separation is crucial to the growth and formation of the vortical patterns.

2. A cylinder undergoing rapid shape change

As a paradigm problem we consider a two-dimensional cylinder of diameter $d_0 = 1.25D$, which is first rapidly accelerated from rest to a steady velocity U, and then rapidly collapsed to a new diameter D. The acceleration and reduction are not coupled.

By restricting the initial acceleration and cylinder shrinking to the time period before flow separation becomes important, we achieve much more clear flow visualizations of the wake patterns following the diameter change; and it is easier to correlate changes in the fluid kinetic energy and vorticity transitions with the body shape change. Since a cylinder must traverse, approximately, a length equal to its diameter before separation is significant, we prescribe the initial acceleration and size reduction to be completed before the cylinder has travelled 40 % of its final diameter. We opted for a rapid 20 % reduction in the cylinder diameter, which provides clear flow visualizations, while retaining the essential features of the problem. Figure 1 provides the kinematics of the cylinder motion and the diameter reduction. In figure 1 the distance the rear-most point on the cylinder has travelled (x_r/D) as a function of time is also plotted. Following the work of Taneda (1977) and others, we use this distance metric as the independent variable throughout the remainder of the work. As shown, the cylinder achieves its final speed when it has travelled $0.05D$, and the size reduction begins when the cylinder has travelled $0.2D$ and is complete at $0.4D$.

We employ two different conditions of shape change. In the first condition, the cylinder is allowed to collapse under prescribed kinematics. This implies that a force is applied that enforces the prescribed motion of the cylinder surface. Fluid from the edges of the flow must enter the domain to replace the space that is emptied by the shrinking cylinder. Also, energy is exchanged between the structure and the fluid, because the kinematics of the collapse is imposed through the application of an external force.

In the second condition, the external surface of the cylinder reduces in a manner kinematically similar to that of a melting cylinder: radial slices sequentially turn into fluid (and hence have initially the same kinetic energy as the moving cylinder). However, no external force is applied to the newly forming fluid layers as they come

https://doi.org/10.1017/jfm.2012.200 Published online by Cambridge University Press

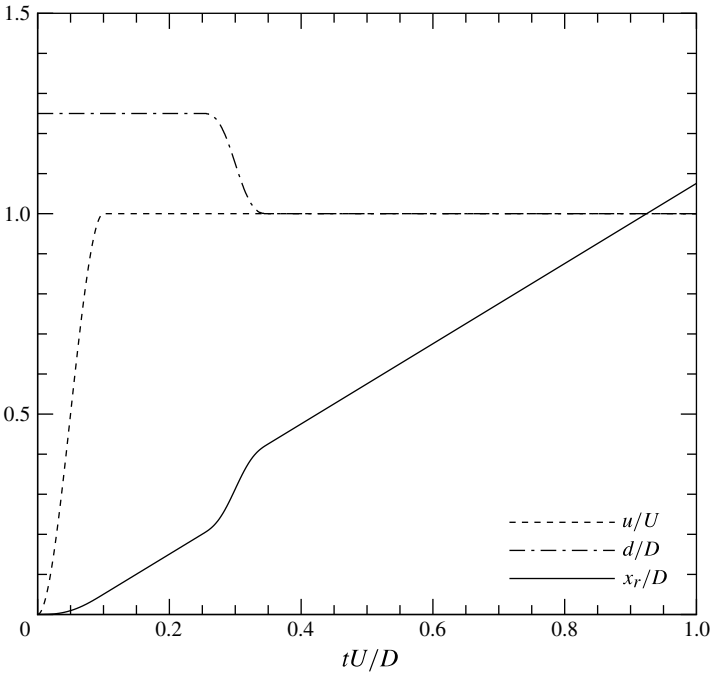


FIGURE 1. Kinematics for the velocity of the centre of the cylinder, u/U, and the diameter, d/D, as function of time. The kinematics was chosen to ensure the acceleration to full speed from rest, and subsequent decrease in diameter, were completed before a significant wake forms. Also shown is the motion of the rearmost point on the cylinder, x_r/D, as the cylinder translates and shrinks. This variable measures the distance the cylinder has travelled, and is used as the independent variable in subsequent figures and throughout the text.

in contact with the surrounding fluid. Hence, the dynamics of the second problem is substantially different than in the first case.

The second case is close to Taylor's problem of the melting disk, except that in our case the body melts only partially. As noted, the second condition is radically different from the first, because there is no external energy input, as no force is applied. Also, it should be noted that the melting applied is not thermodynamic, in the sense that no heat is exchanged and a simple transition from solid to liquid state is assumed.

3. Numerical methodology

For the two-dimensional simulations of the translating and shrinking cylinder we use the boundary data immersion method, a robust immersed boundary method suitable for dynamically deforming bodies with prescribed kinematics. The numerical details of the simulation method follow those in Weymouth *et al.* (2006) and Weymouth & Yue (2011). Briefly, the solid-body dynamic equations and the full nonlinear viscous fluid-dynamic equations are integrated over the solid and fluid domains with a kernel of finite support 2ϵ. This has the effect of blending the equations smoothly over the solid/fluid interface. The integrated equations are valid over the complete domain and allow general solid-body dynamics and solid/fluid interfacial conditions to be applied. The analytic equations are discretized using second-order finite-volume methods in space and Heun's explicit second-order method in time. Previous problems examined with the method include ship flows and flexible-wavemaker flows (Weymouth *et al.*

https://doi.org/10.1017/jfm.2012.200 Published online by Cambridge University Press

2006), solid-body free-surface impact and cavity formation (Weymouth & Yue 2011), as well as shedding of vorticity off a rapidly displaced foil at an angle of attack (Wibawa *et al.* 2012).

All cases in the current viscous study use a no-slip condition for the tangential velocity on the cylinder. The normal-velocity condition for the constant-diameter and collapsing case is a no-penetration condition, i.e. $u_n = v_n$, where v_n is the instantaneous normal velocity of the cylinder wall. This condition has the effect of imposing large forcing on the boundary during collapse, as shown in the following results section. In the melting case, the normal-velocity condition is $u_n = 0$ during the diameter reduction, which imposes no forcing as the cylinder melts.

We consider two different values of the Reynolds number, $Re = 1000$ and 5000, based on the forward speed U and the final diameter D, in order to compare the results. We choose a domain size of $36D \times 24D$ to minimize blockage. A set of four grids was used to establish second-order convergence and approximate the numerical error of the method. The finest grid uses more than 12.5M grid points in the two-dimensional domain and 320 points along the diameter. The coarser grids were generated by skipping every other point in each direction from the previous grid, ensuring that all grids had the same topology. The number of points across the diameter is thus 160, 80 and 40 for the coarse grids. The kernel width is set to $2\epsilon \approx 4\Delta x = D/80$ which is large enough to ensure smooth transition while minimally effecting the near-wall dynamics. For the high-Reynolds-number cases the near-wall boundary layer is not resolved to the levels of direct numerical simulation, and the implicit large-eddy simulation method of Margolin, Rider & Grinstein (2006) is used to model the subgrid-scale effects. The change between the two finest grids in the integrated drag, kinetic energy, and positive circulation was less than 1 % for the $Re = 1000$ cases and less than 2.5 % in the $Re = 5000$ cases. As such we have high confidence in the resolution and accuracy of our simulation of these complex two-dimensional flows.

4. Results

We provide results separately for a cylinder that reduces its size with prescribed kinematics (collapsing cylinder) and a cylinder that melts at a prescribed rate (melting cylinder). The second case is equivalent to a disappearing body, corresponding to the cases, for example, of the shape-changing legs of a duck, or the retracting legs of a water-walking lizard.

For comparison, we first present the resulting flow for a cylinder accelerated from rest to constant speed U, but having constant diameter $d = D$ throughout. Figures 2 and 3 show a sequence of vorticity field images for the speeds corresponding to $Re = 1000$ and $Re = 5000$ respectively. The timing of these images is defined in terms of the distance the cylinder has travelled (x_r/D), which is given as a function of time in figure 1. All figures are shown relative to the translating body centre, x_c. As shown in these figures, the vortex shedding does not occur until x_r is greater than one diameter for either case. The drag, kinetic energy, and circulation of these flows are presented with the comparison to the shrinking cases in the next two subsections.

4.1. *First case: collapsing cylinder*

As described in § 2, the first case is that of a collapsing cylinder; the fluid is required to maintain the no-slip boundary condition at all times. The kinematics of the cylinder surface during collapse are prescribed, as shown in figure 1, and a force is required at the cylinder–fluid interface to enforce these kinematics.

https://doi.org/10.1017/jfm.2012.200 Published online by Cambridge University Press

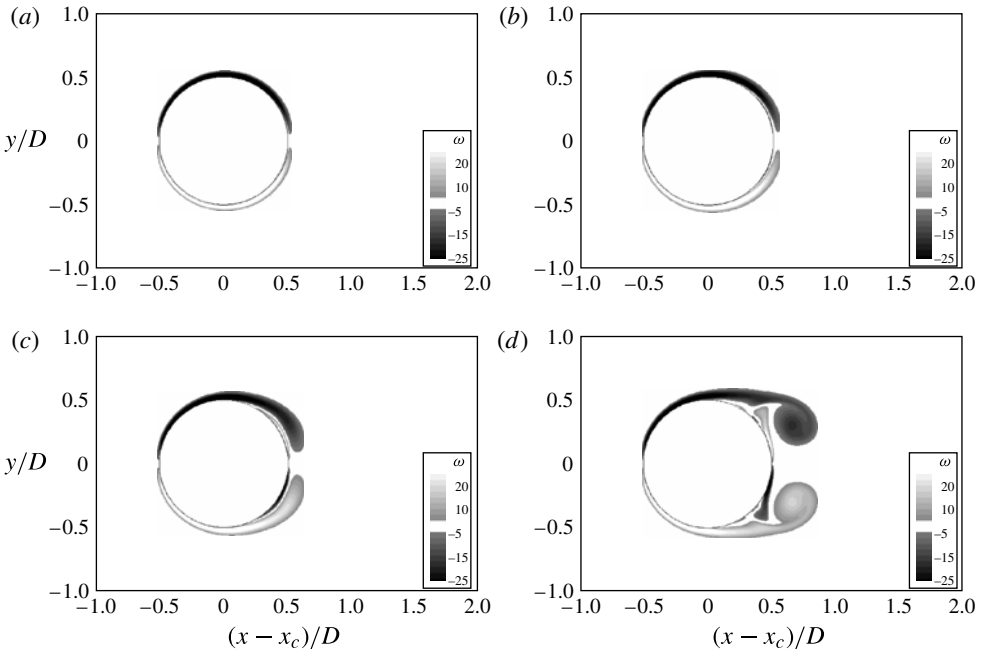


FIGURE 2. Vorticity (ω) contours for the constant-diameter cylinder as a function of the distance travelled x_r/D: (*a*) $x_r/D = 0.2$; (*b*) $x_r/D = 0.4$; (*c*) $x_r/D = 0.8$; (*d*) $x_r/D = 1.6$. The flow undergoes significant separation only after $x_r/D > 1$ as shown in (*d*) by which time two symmetric vortices have formed. $Re = 1000$:

Figure 4 shows a sequence of vorticity images before and after the reduction phase for a final speed and diameter providing a Reynolds number of $UD/\nu = 1000$. As shown, during the phase of diameter resizing (x_r/D between 0.2 and 0.4) a thickening of the boundary layer is observed, while some separation occurs in the rear of the cylinder. This is shown more clearly in figure 5(*a*), which highlights the reversed-flow region on the top half of the cylinder at $x_r/D = 0.4$. Figure 5(*b*) plots the surface pressure on the cylinder during resizing, relative to the leading-edge stagnation pressure. As shown on the figure, a large positive pressure gradient develops on the cylinder walls during shrinking (between $tU/D = 0.25$ and $tU/D = 0.35$), which causes the reversed flow and the generation of opposite-signed vorticity on the cylinder wall.

We now proceed to explain why reducing the cylinder diameter, a process which within potential flow we can model as the addition of an irrotational sink, causes reversed flow on the cylinder. First, we consider the potential flow analogy to the cylinder system before shrinking, consisting of a dipole and a uniform flow; the velocity field and kinetic energy per unit mass (which is proportional to the relative pressure) are given in cylindrical coordinates (r, θ) by

$$u_r = \left(U - \frac{\mu}{r^2}\right)\cos\theta, \tag{4.1}$$

$$u_\theta = -\left(U + \frac{\mu}{r^2}\right)\sin\theta, \tag{4.2}$$

$$\kappa = \frac{U^2}{2} - \frac{U\mu}{r^2}\cos(2\theta) + \frac{\mu^2}{2r^4}. \tag{4.3}$$

https://doi.org/10.1017/jfm.2012.200 Published online by Cambridge University Press

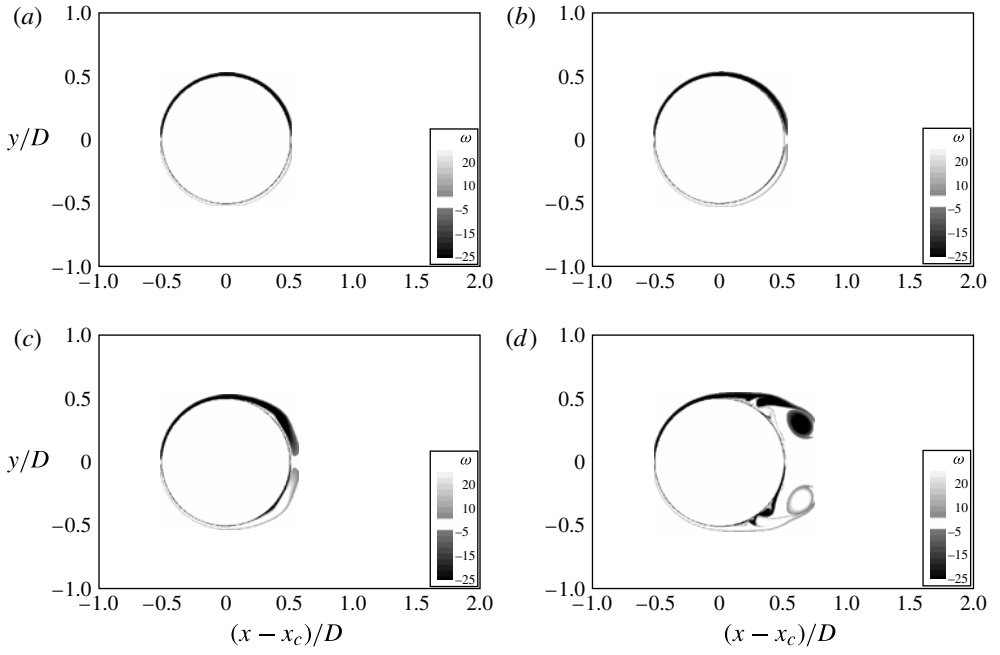


FIGURE 3. As figure 2 but for $Re = 5000$. The higher Reynolds number adds complexity to the vortex structures but does not change the time for significant vortex formation: (*a*) $x_r/D = 0.2$; (*b*) $x_r/D = 0.4$; (*c*) $x_r/D = 0.8$; (*d*) $x_r/D = 1.6$.

Proceeding to the diameter-collapsing phase, the superposition of a sink gives the new form of the equations as

$$u_r = \frac{\alpha}{r} + \left(U - \frac{\mu}{r^2}\right)\cos\theta, \tag{4.4}$$

$$u_\theta = -\left(U + \frac{\mu}{r^2}\right)\sin\theta, \tag{4.5}$$

$$\kappa = \kappa_{cylinder} + \frac{\alpha^2}{2r^2} + \frac{\alpha}{r}\left(U - \frac{\mu}{r^2}\right)\cos\theta, \tag{4.6}$$

where we find a new θ-dependent term in the kinetic energy, with opposite sign and half the wavenumber as the one in the original cylinder flow. This matches the behaviour of the relative surface pressure in figure 5(*b*) and indicates that this nonlinear combination of forward motion and reduction drives the flow reversal.

In figure 6 we compare the integrated non-dimensionalized pressure drag force, total positive-sign vorticity (defined as the area integral of the positive vorticity, namely $\Omega^+ \equiv \int \max(\omega, 0)\,\mathrm{d}v$, i.e. the vorticity on the upper half of the cylinder) and integrated kinetic energy, $T = \int \kappa\,\mathrm{d}v$, for the three cases of a cylinder with constant diameter D, the collapsing cylinder, and the melting cylinder to be discussed in § 4.2. Our kinetic energy metric includes the energy of both the fluid and the cylinder to account for the change in solid-body energy when the cylinder changes size. Normalizing by the final cylinder energy $T_c = (1/2)\rho\pi D^2 U^2$ gives $T/T_c = 2$ as the potential flow prediction, matching our initial constant-diameter result. Note that

https://doi.org/10.1017/jfm.2012.200 Published online by Cambridge University Press

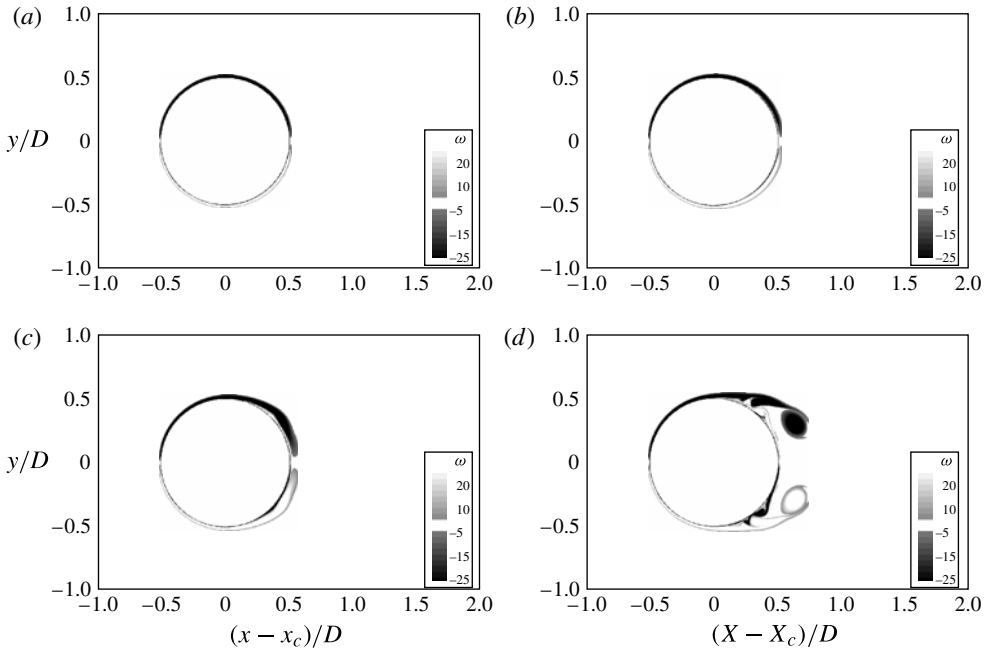


FIGURE 4. Vorticity contours in the collapsing cylinder flow just before ($x_r/D = 0.2$) and after ($x_r/D \geqslant 0.4$) the phase of diameter reduction: (*a*) $x_r/D = 0.2$; (*b*) $x_r/D = 0.4$; (*c*) $x_r/D = 0.8$; (*d*) $x_r/D = 1.6$. In (*d*) the flow has separated forming two symmetric vortices. $Re = 1000$.

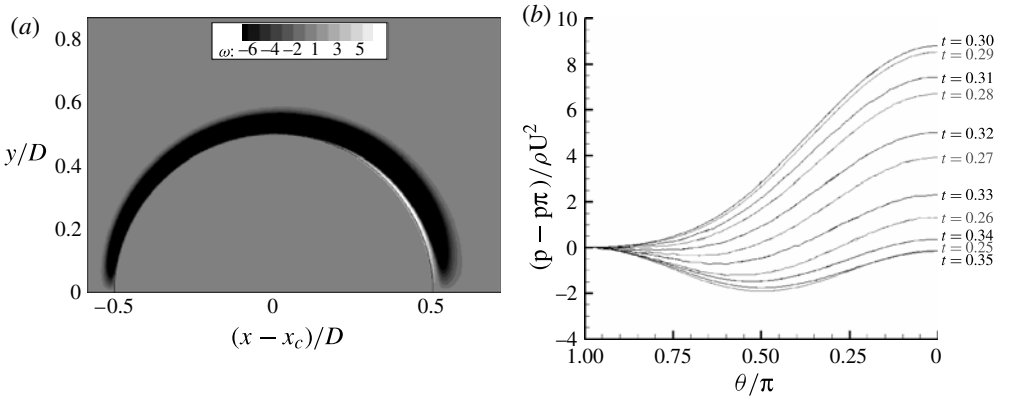


FIGURE 5. (*a*) Vorticity, and (*b*) surface pressure during the cylinder collapse, $Re = 1000$. Vorticity is shown at $x_r/D = 0.4$ ($tU/D = 0.35$) with the view and contour levels zoomed-in to highlight the white reversed flow region. The surface pressure is shown relative to the leading-edge stagnation pressure at $\theta = \pi$.

the potential flow prediction for the kinetic energy for the size change cases are 56 % larger ($T/T_c = 2 \times 1.25^2 = 3.125$) because of the larger initial diameter $d_0 = 1.25D$ in these cases. Again, the measured kinetic energy in figure 6 matches this potential flow prediction quite closely.

https://doi.org/10.1017/jfm.2012.200 Published online by Cambridge University Press

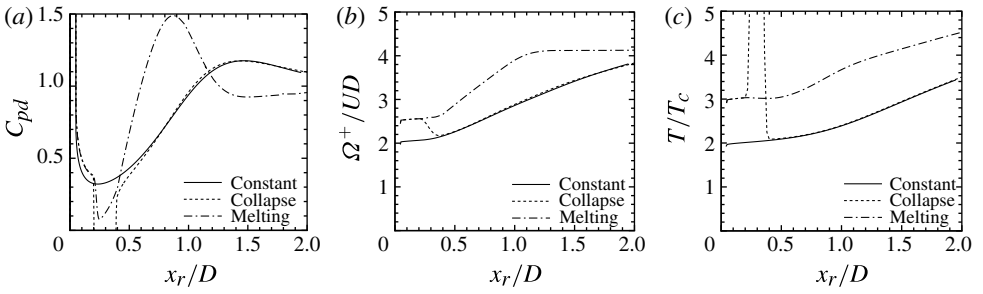


FIGURE 6. (*a*) The integrated pressure drag force, (*b*) positive-sign vorticity, and (*c*) kinetic energy (including the cylinder's kinetic energy) for three test cases: a cylinder with constant diameter D (solid lines); the collapsing cylinder of § 4.1 (dotted line); and the melting cylinder of § 4.2 (dashed line) at $Re = 1000$.

Examining figure 6 for the collapsing-cylinder case, during the diameter-shrinking phase we find that:

(*a*) the cylinder experiences a large positive thrust force;

(*b*) there is a gradual reduction in the positive total vorticity on the uper half of the cylinder and a corresponding reduction in negative total vorticity on the other half of the cylinder, due to cancellation with the opposite-sign vorticity generated at the wall; and

(*c*) there is a spike in kinetic energy due to the influx of fluid from the far field to fill in the space created by the collapsing cylinder.

The thrust force is caused by the pressure gradient shown in figure 5, and peaks at $C_{pd} = -16.6$ making it too large to effectively show in figure 6(*a*). We can attribute the large thrust force F_{pd} to the effect of reducing the mass M and added mass M_a during the collapse, i.e. $F_{pd} = U\,(\mathrm{d}/\mathrm{d}t)(M + M_a)$. For the imposed kinematics this gives a maximum estimated potential flow thrust coefficient of $C_{pd} = -17.5$, only 5 % greater than the value calculated in our viscous flow.

After the size change is complete, the vorticity fields for the reduced cylinder in figure 4(*c*,*d*) match closely those of the constant-diameter cylinder in figure 2(*c*,*d*). Figure 6(*c*) shows that the kinetic energy of the fluid decreases after the collapse due to the forcing applied on the cylinder boundary during the collapse, which recovers the difference in energy due to the change in the added mass. Indeed, following the diameter-shrinking phase, all quantities are remarkably close to those for a cylinder with constant diameter, equal to the reduced value D.

Figures 7 and 8, provide the same data as figures 4 and 6 but at the higher Reynolds number of 5000. For the higher Reynolds number there are some relatively small differences in the dynamics of the boundary layer, but, overall, there is close similarity with the results at $Re = 1000$. Figure 8 provides the drag force, total positive-sign vorticity, and kinetic energy for the higher Reynolds number $Re = 5000$. Compared with figure 6, we find close agreement qualitatively, and only moderate differences quantitatively, attributable to differences in the shedding process due to the Reynolds number effects.

In conclusion, the viscous simulation provides results in agreement with potential flow prediction, including fluid energy recovery as the differential in the kinetic energy of the fluid associated with the smaller added mass is taken back at the surface of

https://doi.org/10.1017/jfm.2012.200 Published online by Cambridge University Press

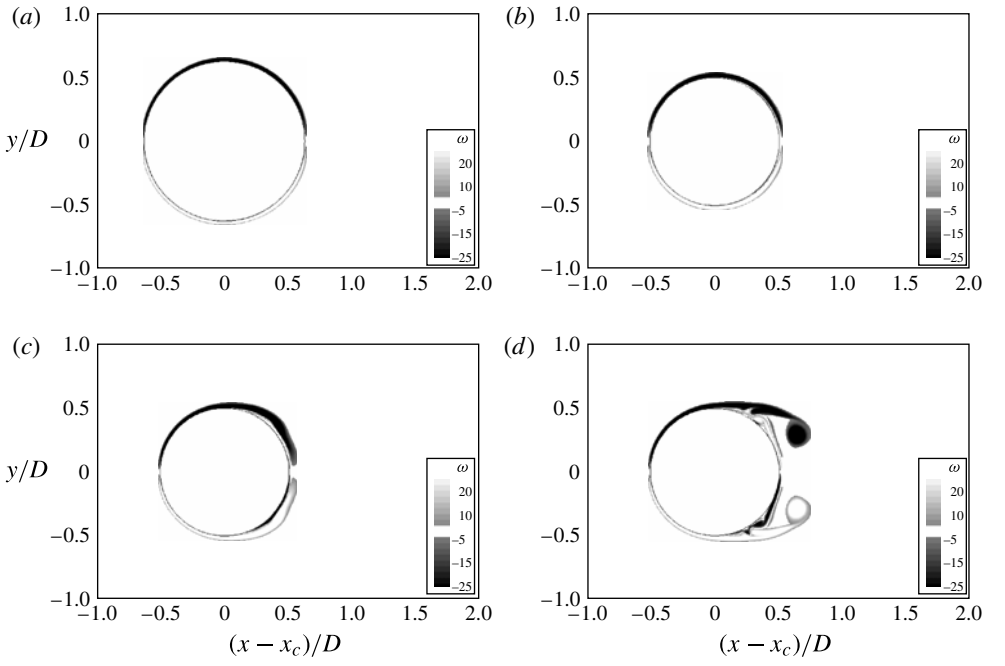


FIGURE 7. Vorticity contours for the collapsing cylinder at the higher Reynolds number, $Re = 5000$, for the same x_r/D positions as in figure 4: (*a*) $x_r/D = 0.2$; (*b*) $x_r/D = 0.4$; (*c*) $x_r/D = 0.8$; (*d*) $x_r/D = 1.6$.

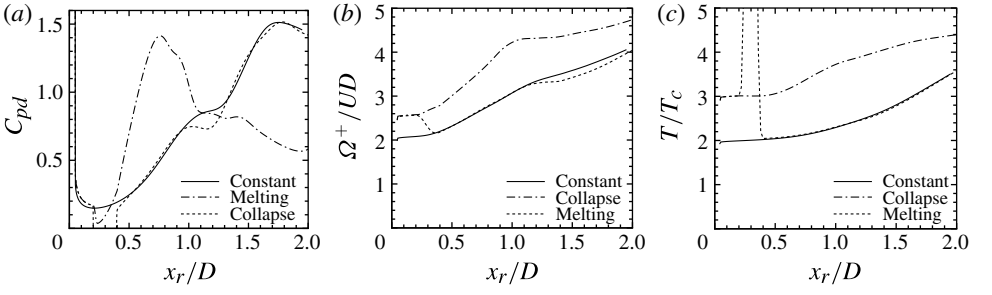


FIGURE 8. (*a*) The integrated pressure drag force, (*b*) total positive-sign vorticity, and (*c*) kinetic energy (including the cylinder's kinetic energy) at $Re = 5000$ for the same cases as in figure 6.

the body during the prescribed collapse. A reduction in total boundary layer vorticity on the upper (and lower) side of the cylinder is achieved through annihilation with opposite-sign vorticity, generated during the collapse.

4.2. *Second case: 'melting' cylinder*

As described in § 2, the diameter reduction in the second case is achieved through a rapid but orderly 'melting' of the cylinder walls, in the sense that circular outer layers of the cylinder turn successively into fluid, starting from the outer diameter $d_0 = 1.25D$ and proceeding until a new diameter, D, is reached. While we will refer to this process

https://doi.org/10.1017/jfm.2012.200 Published online by Cambridge University Press

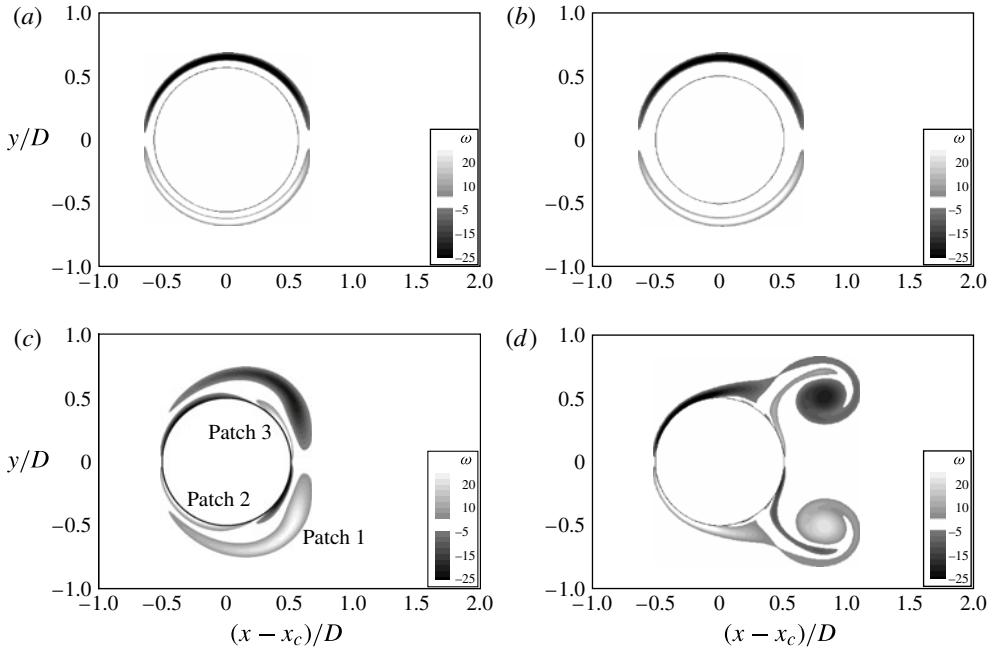


FIGURE 9. Vorticity contours for the melting cylinder case during and after melting, $Re = 1000$: (*a*) $x_r/D = 0.3$; (*b*) $x_r/D = 0.4$; (*c*) $x_r/D = 0.8$; (*d*) $x_r/D = 1.6$. In (*c*) the main patches of positive vorticity tracked in figure 11 are labelled.

as melting, it is not meant to be a thermodynamic process, but a simple change from solid to liquid phase without heat exchange. The cylinder surface kinematics for this second case are the same as in § 4.1, as plotted in figure 1, but the dynamics are completely changed. No external force is applied throughout this phase to the melting layers, which at the time of 'melting' retain their initial kinetic energy, i.e. they have the same kinetic energy per unit volume as the moving cylinder.

Figures 9 and 10 provide a sequence of images of the vorticity and kinetic energy of the flow, respectively, during and after the melting phase, for a Reynolds number of 1000 based on the final diameter. Before melting (for $x_r/D \leqslant 0.2$) the flow is identical to the collapsing cylinder case of § 4.1, but after that point there are significant differences: it is clearly seen that the initial vorticity of the boundary layer is instantaneously shed in the fluid during melting; subsequently, within a short time, the vorticity from the upper and lower sides forms rapidly a pair of large, strong vortices, while secondary vorticity forms, to satisfy the no-slip condition at the surface of the cylinder. As the shed vorticity reshapes into free vortices, a new boundary layer develops on the reduced walls of the cylinder.

To quantify the vorticity and kinetic energy shed into the fluid, we track the individual patches of vorticity as defined by the $|\omega|D/U = 6$ contours lines. This level was chosen as the lowest value that provided a continuous separation between the shed and re-establishing boundary layer. Defining a patch of vorticity by a fixed contour level is not exact, as viscosity will cause vorticity to continually diffuse outside this level, as time progresses. However, it does give a fairly good indication of the relative size and strength of these complex, non-uniform vorticity patches.

https://doi.org/10.1017/jfm.2012.200 Published online by Cambridge University Press

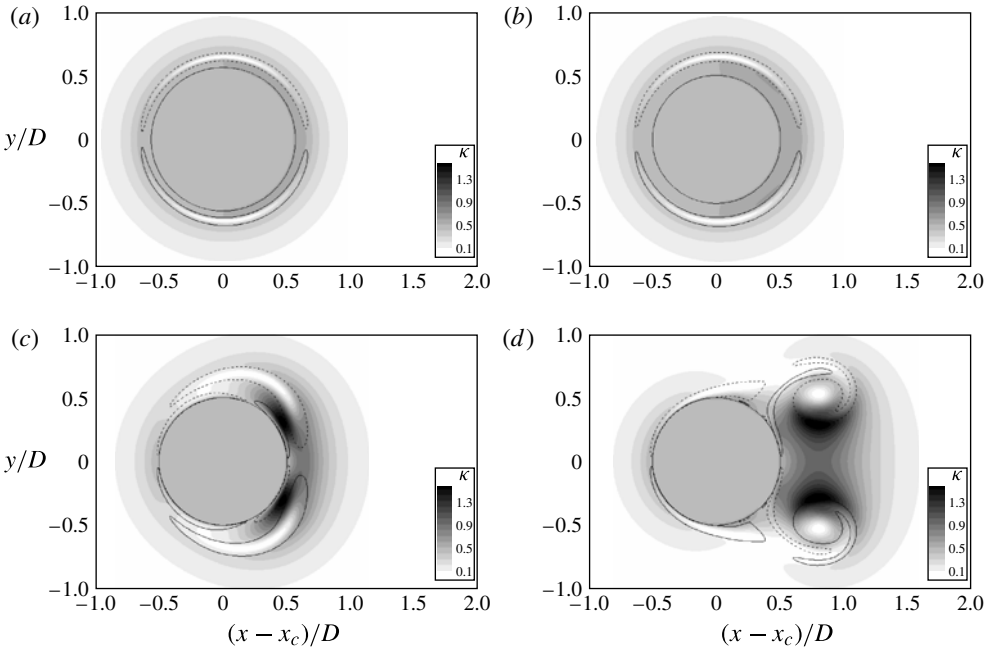


FIGURE 10. Kinetic energy contours for the melting cylinder flow at $Re = 1000$ with the $|\omega|D/U = 6$ contour lines overlaid: (*a*) $x_r/D = 0.3$; (*b*) $x_r/D = 0.4$; (*c*) $x_r/D = 0.8$; (*d*) $x_r/D = 1.6$.

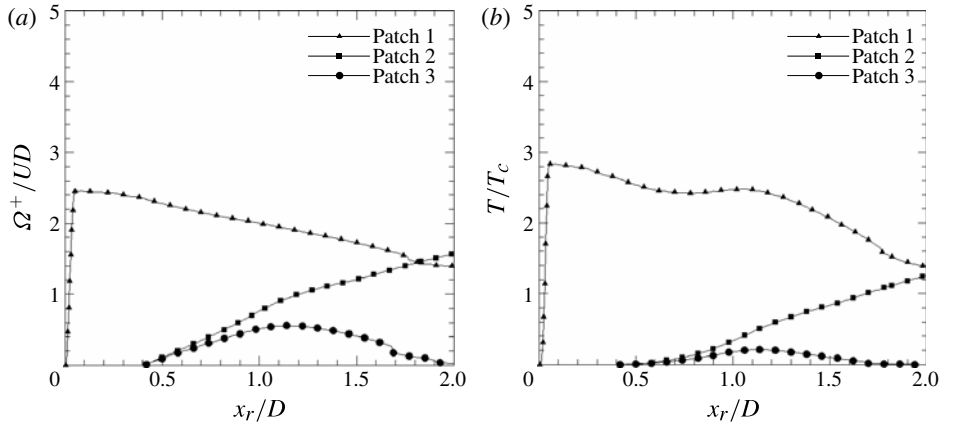


FIGURE 11. (*a*) The integrated positive-sign vorticity and (*b*) effective kinetic energy for the main patches of vorticity labelled in figure 9(*c*) for the melting cylinder case, $Re = 1000$.

As labelled in figure 9(*c*), we will denote the shed vorticity generated in the original boundary layer (before melting starts) as patch 1, the re-establishing boundary layer on the reduced diameter cylinder as patch 2, and the secondary vorticity formed to satisfy the no-slip condition on the cylinder as patch 3. Note that each of these patches has a mirror-image with opposite-sign vorticity on the other side of the cylinder.

https://doi.org/10.1017/jfm.2012.200 Published online by Cambridge University Press

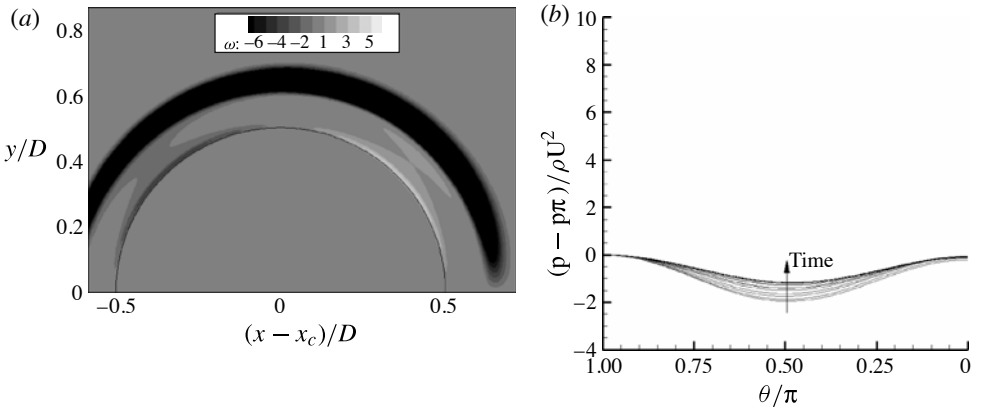


FIGURE 12. Vorticity (*a*) and relative surface pressure (*b*) during the cylinder melting, $Re = 1000$. The same times, levels, and scales are used as in figure 5. (*a*) Shows the initial stages of the secondary vorticity generated at the wall by the shed vorticity. In contrast to the collapsing case, the pressure for the melting case increases only slightly, predominantly at the midpoint $\theta = \pi/2$.

We calculate the vorticity for each positive circulation patch 1, 2, and 3. Also, we calculate an *effective kinetic energy* for each patch, defined as the kinetic energy of each patch and its mirror image in the fluid, but in the absence of the remaining patches and the cylinder; this is simply a helpful metric to follow the changes in kinetic energy. The vorticity and effective kinetic energy are shown in figure 11. As shown, the positive-sign vorticity of patch 1 remains constant up to about $x_r/D = 0.5$, and then declines very slowly thereafter. Likewise, the kinetic energy remains nearly constant within patch 1 up to $x_r/D = 1.0$. As shown in figures 6 and 8, the total energy remains constant up to at least $x_r/D = 0.7$, well beyond the melting phase; hence nearly the entire change in added mass energy is contained in the forming eddies.

Referring back to figure 6, the dynamics of the melting process has a strong effect on the integrated force, total positive vorticity and kinetic energy compared to both the constant-diameter and collapsing cylinder test cases. During melting, the drag coefficient drops nearly to zero. This effect is shown in more detail in figure 12, which plots the vorticity and relative surface pressure using the same scales as figure 5. Unlike the collapsing case, the melting cylinder experiences only a slight increase in the pressure from the mid-body to the rear stagnation point. The melting fluid is sheltering the surface of the body from the external flow, reducing the shear and pressure drop on the body. After melting is complete, figure 6 shows that the drag force rises quickly as the two vortices form and the near-wall flow re-establishes, reaching a peak around $x_r/D = 0.85$, and then decreasing as the vortices are shed in the wake.

The kinetic energy is constant, remaining near the potential flow prediction of $T/T_c = 3.1$ throughout melting, because energy is simply transferred from the body to the fluid, with no change to the total energy. After melting, the re-establishing boundary layer on the cylinder adds significantly to the total positive vorticity and kinetic energy.

https://doi.org/10.1017/jfm.2012.200 Published online by Cambridge University Press

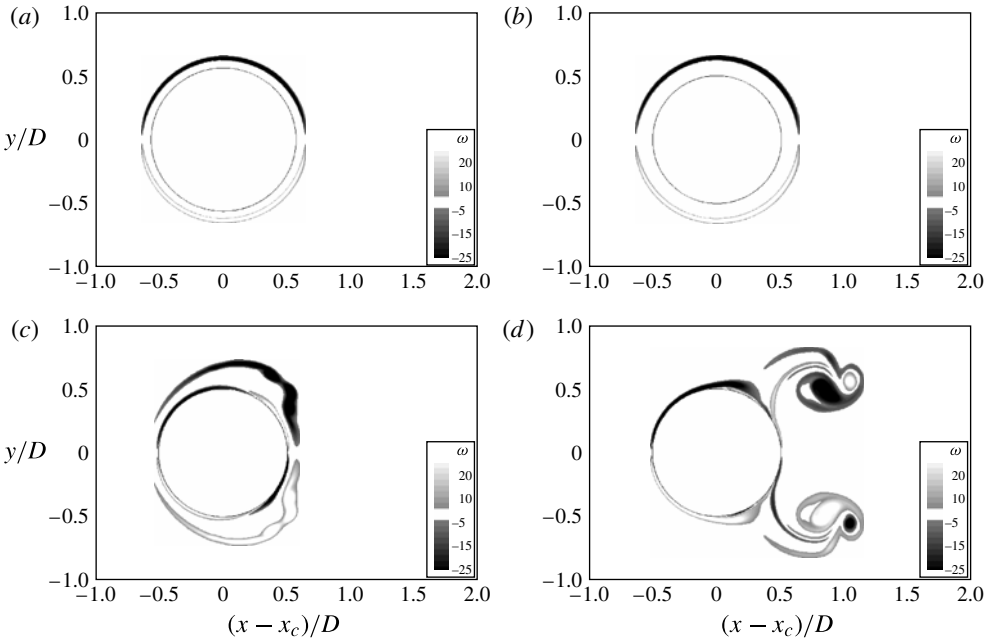


FIGURE 13. Vorticity contours in the melting cylinder flow at $Re = 5000$ during and after melting: (*a*) $x_r/D = 0.3$; (*b*) $x_r/D = 0.4$; (*c*) $x_r/D = 0.8$; (*d*) $x_r/D = 1.6$.

Figures 13, 14 and 8 provide the same data for the higher Reynolds number of 5000. While at the higher Reynolds number the flow patterns are more complex, primarily during the evolution of the shed vorticity, the overall behaviour is nearly the same as at the lower Reynolds number.

5. Discussion

The principal goal of the paper is to study the transition of boundary layer vorticity and the change in fluid kinetic energy for a vanishing cylinder. We focused on the two-dimensional flow of a steadily translating circular cylinder undergoing a significant reduction in diameter, because it is geometrically simple and efficient to calculate, but nonetheless contains all the basic elements of the vanishing-body problem. By studying two different ways of changing the shape, the first consisting of a collapse of the cylinder under prescribed kinematics, enforced by external forcing; and the second consisting of a prescribed, sequential melting of the outer cylinder surface, we obtained radically different flow patterns in each case.

Considering first the problem of a collapsing cylinder under prescribed kinematics, requiring the application of a force at the cylinder surface, the reduction in diameter results in a corresponding reduction of the fluid kinetic energy and the fluid momentum associated with the cylinder added mass; the external forcing applied during collapse causes the energy difference to be absorbed at the surface of the cylinder, as potential flow predicts. The vorticity on each half of the cylinder is also reduced during collapse. As investigated in such works as Morton (1984) and Hunt & Eames (2002), annihilation with opposite-sign vorticity is the only mechanism for reduction of vorticity. In this problem the reversed flow on the wall of the collapsing

https://doi.org/10.1017/jfm.2012.200 Published online by Cambridge University Press

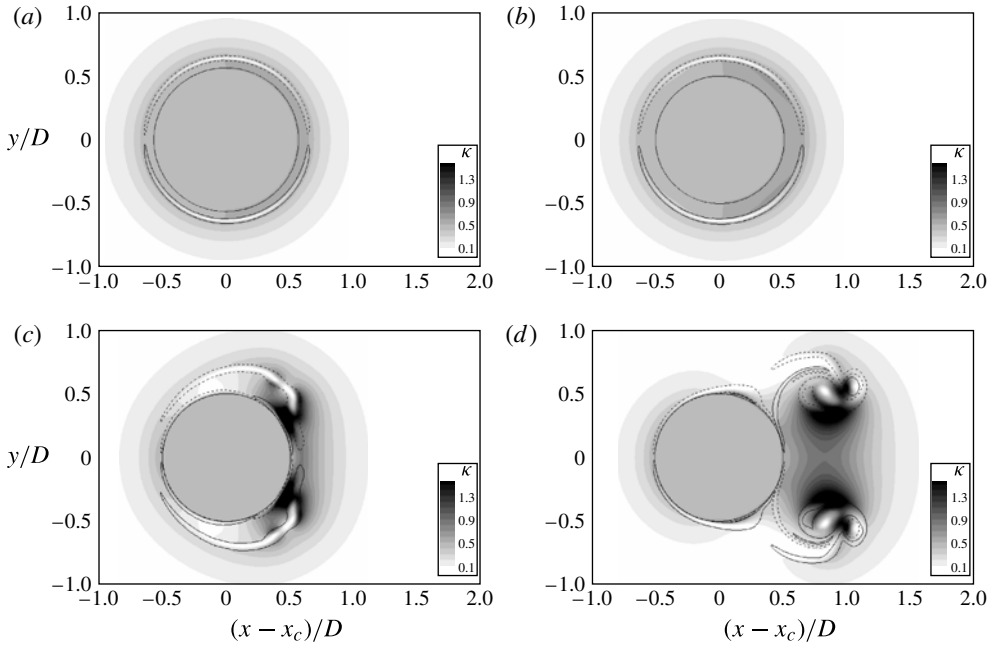


FIGURE 14. Kinetic energy contours with $|\omega|D/U = 6$ contours lines overlaid on the melting cylinder flow at $Re = 5000$: (*a*) $x_r/D = 0.3$; (*b*) $x_r/D = 0.4$; (*c*) $x_r/D = 0.8$; (*d*) $x_r/D = 1.6$.

cylinder generates the opposite-sign vorticity which annihilates the boundary layer vorticity that had formed prior to the collapse. The interesting result for this case, as figure 4 clearly shows, is that after collapse the flow is qualitatively and quantitatively the same as the flow around a constant-diameter cylinder accelerated from rest, despite the process of reduction in size. Hence, the flow retains practically no memory of the larger initial size and fluid kinetic energy, and the finally forming flow patterns and shed vortices match those of the smaller diameter cylinder.

The 'melting' cylinder problem models a vanishing body, and hence it has implications for the locomotion of animals that employ retracting or rapidly varying fins or limbs. The basic difference with the collapsing cylinder is that during the disappearance of the body there is no external force acting at the interface of the body and the fluid, and hence the boundary layer vorticity, as well as part of the fluid kinetic energy and momentum, are shed in the flow. Figure 9 depicts a flow with sharply contrasting features relative to figure 4. The vorticity in the boundary layer, formed prior to the melting phase, is shed in the fluid and rolls up to form two vortices, which are far larger at $x_r/D = 1.6$ than the corresponding vortices obtained at the same time in figure 2 for the constant diameter cylinder. It should also be noted that the peak drag force is reached within a very short time after the melting process, as the two large vortices form and are shed in the wake; the peak force is reached at $x_r/D \approx 0.80$, whereas the peak force in a rigid cylinder is reached at $x_r/D = 1.5$ at $Re = 1000$ and $x_r/D = 1.8$ at $Re = 5000$ (see figures 6 and 8). The rise time for a melting cylinder, defined as the time from the minimum to the maximum values in the drag coefficient, corresponds to $\delta x_r/D = 0.4$, while for a rigid or collapsed cylinder $\delta x_r/D$ ranges from a rise time of 1.2 at $Re = 1000$, to a value of 1.6 at $Re = 5000$.

https://doi.org/10.1017/jfm.2012.200 Published online by Cambridge University Press

Figure 11 shows that the vorticity associated with 'patch 1', defined in figure 9(*c*) to be the boundary layer vorticity shed during melting, rolls up eventually into the vortex shed by the cylinder, as shown at $x_r/D = 1.6$. The total vorticity and kinetic energy of patch 1 remains roughly constant; both quantities are decreasing mildly up to $x_r/D = 1.2$ when opposite-sign vorticity from patch 3 is entrained, reducing the circulation of the vortex. Patch 3 is defined in figure 9(*c*) as the secondary vorticity generated over the cylinder surface following the melting phase, and is induced by the presence of patch 1.

The studies by Taylor (1953), and Fohl (1968) employ inviscid flow theory and assume that the 'bound' vorticity released in the flow will subsequently concentrate to form either two vortices when a cylinder dissolves, or a vortex ring in the case of a dissolving sphere or disk; and no significant other patterns will form. This is a working hypothesis that inviscid flow cannot resolve. In the present study we show through viscous simulation of a melting cylinder that indeed the principal pattern forming in the wake is a pair of strong vortices. We also find through simulation at two different Reynolds numbers that the thickness of the boundary layer does not affect the form of the vortical patterns. We show that this is true even for a partially melting cylinder, and show that the difference in the kinetic energy associated with the added mass of the cylinder is contained in the forming vortex pair. As in the inviscid flow predictions of Eames (2008*b*) we find that the kinetic energy is conserved during melting.

There are two principal results of this study.

(*a*) We show that strong vortices form rapidly when a moving body partially vanishes (or 'melts'), which contain the body boundary layer vorticity formed before melting, as well as the difference in kinetic energy due to the change in added mass. The time taken to form these vortices is between one-third and one-fourth of the time required for a rigid translating cylinder to shed vortices. Such strong vortices can be used within unsteady flows to control the flow or generate forces for propulsion or manoeuvring. Rapid shape change in a periodic motion, for example, can generate forces rapidly in one direction only. Alternatively, a rapidly vanishing body can generate vortices that impinge on another body to alter the flow or generate forces in a short time interval (Rockwell 1998).

(*b*) We show that for a collapsing body, the change in kinetic energy due to the difference in added mass can be recovered, while vorticity dynamics are of secondary importance. Hence, for example, in a periodically deflating and inflating body, equipped with the capability to store energy, the change of shape need not be energetically costly, because added mass energy is clearly recoverable, as potential flow would predict. For example, if the muscles of a periodically shape-varying animal, or the actuators of a fish-like device contain spring-like elements, they can store the recovered energy during the deflation stage, and then release it during the inflation stage.

The results at two Reynolds numbers, $Re = 1000$ and $Re = 5000$, are shown to be qualitatively the same and quantitatively similar.

6. Conclusions

Rapid change of the diameter of a steadily moving two-dimensional circular cylinder is used as a model to study the effects of body shape on the fluid patterns and forces acting on vanishing or deforming bodies.

https://doi.org/10.1017/jfm.2012.200 Published online by Cambridge University Press

When the cylinder collapses rapidly under prescribed kinematics, it is shown that the difference in fluid kinetic energy can be recovered at the cylinder–fluid interface, while opposite-sign vorticity is generated on the upper and lower halves of the cylinder, and reduces the vorticity formed before collapse. The overall process differs little from what potential flow predicts, and allows energy recovery; this has significant implications, for example, for the energetics of bodies undergoing periodic inflation and deflation stages.

When the cylinder undergoes an orderly but rapid 'melting', whereby the outer cylinder layer transitions from solid to fluid state, the boundary layer vorticity is shed in the fluid globally and rapidly, forming a pair of vortices that contain and transport the excess kinetic energy. The radically different flow patterns, relative to both a rigid cylinder and a deflating cylinder, also outline a different model mechanism for the rapid generation of large vortical patterns in the fluid through body vanishing: the time to form the vortices is only a fraction of the time that a rigid cylinder takes to form such vortices.

Acknowledgements

The authors wish to acknowledge support from the Singapore–MIT Alliance for Research and Technology, and from the MIT Sea Grant Program.

REFERENCES

CHILDRESS, S., VANDENBERGHE, N. & ZHANG, J. 2006 Hovering of a passive body in an oscillating airflow. *Phys. Fluids* **18**, 117103.

DABIRI, J. O. 2005 On the estimation of swimming and flying forces from wake measurements. *J. Expl Biol.* **208**, 3519–3532.

DICKINSON, M. 2003 Animal locomotion: how to walk on water? *Nature* **424**, 621–622.

DONG, H., BOZKURTTAS, M., MITTAL, R., MADDEN, P. & LAUDER, G. V. 2010 Computational modelling and analysis of the hydrodynamics of a highly deformable fish pectoral fin. *J. Fluid Mech.* **645**, 345–373.

DRUCKER, E. G & LAUDER, G. V. 2000 A hydrodynamic analysis of fish swimming speed: wake structure and locomotor force in slow and fast labriform swimmers. *J. Expl Biol.* **203**, 2379–2393.

EAMES, I. 2008*a* Disappearing bodies and ghost vortices. *Phil. Trans. R. Soc. Lond.* A **366**, 2219–3232.

EAMES, I. 2008*b* Rapidly dissolving dense bodies in an inviscid fluid. *Proc. R. Soc. Lond.* A **464**, 2985–3002.

FOHL, T. 1968 The creation of vortex rings by impulsive acceleration of a sphere of fluid. *J. Appl. Phys.* **39**, 2470–2471.

HEDENSTROM, A., JOHANSSON, L. C. & SPEDDING, G. R. 2006 Bird or bat: comparing airframe design and flight performance. *Bioinsp. Biomim.* **4**, 015001.

HSIEH, S. T. & LAUDER, G. V. 2004 Running on water: three-dimensional force generation by basilisk lizards. *Proc. Natl Acad. Sci.* **101**, 16787.

HU, D. L. & BUSH, J. W. M. 2010 The hydrodynamics of water-walking arthropods. *J. Fluid Mech.* **644**, 5–33.

HUNT, JCR & EAMES, I. 2002 The disappearance of laminar and turbulent wakes in complex flows. *J. Fluid Mech.* **457**, 111–132.

JOHANSSON, L. C. & NORBERG, U. M. L. 2001 Lift-based paddling in diving grebe. *J. Expl Biol.* **204**, 1687–1696.

JOHANSSON, L. C. & NORBERG, R. A. 2003 Delta-wing function of webbed feet gives hydrodynamic lift for swimming propulsion in birds. *Nature* **424**, 65–68.

KANSO, E. 2009 Swimming due to transverse shape deformations. *J. Fluid Mech.* **631**, 127–148.

https://doi.org/10.1017/jfm.2012.200 Published online by Cambridge University Press

LENTINK, D., MÜLLER, U. K., STAMHUIS, E. J., DE KAT, R., VAN GESTEL, W., VELDHUIS, L. L. M., HENNINGSSON, P., HEDENSTRÖM, A., VIDELER, J. J. & VAN LEEUWEN, J. L. 2007 How swifts control their glide performance with morphing wings. *Nature* **446**, 1082–1085.

LINDHE NORBERG, U. M. & WINTER, Y. 2006 Wing beat kinematics of a nectar-feeding bat, Glossophaga soricina, flying at different flight speeds and Strouhal numbers. *J. Expl Biol.* **209**, 3887–3897.

MARGOLIN, L. G., RIDER, W. J. & GRINSTEIN, F. F. 2006 Modelling turbulent flow with implicit LES. *J. Turbul.* **7**, 1–27.

MCHENRY, M. J. & JED, J. 2003 The ontogenic scaling of hydrodynamics and swimming jellyfish (Aurelia aurita). *J. Expl Biol.* **206**, 4125–4137.

MORTON, B. R. 1984 The generation and decay of vorticity. *Geophys. Astrophys. Fluid Dyn.* **28**, 277–308.

MULLER, U. K. & LENTINK, D. 2004 Physiology - Turning on a dime. *Science* **306**, 1899–1900.

RAMAMURTI, R., SANDBERG, W. C., LOHNER, R., WALKER, J. A. & WESTNEAT, M. W. 2002 Fluid dynamics of aquatic flight in the bird wrasse: three dimensional unsteady computations with fin deformation. *J. Expl Biol.* **205**, 2997–3008.

ROCKWELL, D. 1998 Vortex–body interactions. *Annu. Rev. Fluid Mech.* **30**, 199–229.

SPAGNOLIE, S. E. & SHELLEY, M. J. 2009 Shape-changing bodies in fluid: hovering, ratcheting, and bursting. *Phys. Fluids* **21**, 013103.

TANEDA, S. 1977 Visual study of unsteady separated flows around bodies. *Prog. Aerosp. Sci.* **17**, 287–348.

TAYLOR, G. I. 1953 Formation of a vortex ring by giving an impulse to a circular disk and then dissolving it away. *J. Appl. Phys.* **24**, 104.

WEYMOUTH, G. D., DOMMERMUTH, D. G., HENDRICKSON, K. & YUE, D. K.-P. 2006 Advancements in Cartesian-grid methods for computational ship hydrodynamics. In *Proceedings of the 26th Symposium on Naval Hydrodynamics, Rome, Italy*, pp. 17–22 September.

WEYMOUTH, G. D. & YUE, D. K.-P. 2011 Boundary data immersion method for Cartesian-grid simulations of fluid–body interaction problems. *J. Comput. Phys.* **230**, 16.

WIBAWA, M. S., STEELE, S. C., DAHL, J. D., RIVAL, D. E., WEYMOUTH, G. D. & TRIANTAFYLLOU, M. S. 2012 Global vorticity shedding for a vanishing wing. *J. Fluid Mech.* **695**, 112–134.

WILLIAMSON, C. H. K. 1996 Vortex dynamics in the cylinder wake. *Annu. Rev. Fluid Mech.* **28**, 477–539.

https://doi.org/10.1017/jfm.2012.200 Published online by Cambridge University Press